Sensors & Actuators: B. Chemical 280 (2019) 54–61

Contents lists available at ScienceDirect

Sensors and Actuators B: Chemical

journal homepage: www.elsevier.com/locate/snb

Functionalized gold electroless-plated optical fiber gratings for reliable surface biosensing

Médéric Loyez[a], Clotilde Ribaut[a,b], Christophe Caucheteur[b,*], Ruddy Wattiez[a]

[a] Proteomics and Microbiology Department, Université de Mons, Champ de Mars 6, 7000 Mons, Belgium
[b] Electromagnetism and Telecommunication Department, Université de Mons, Bld Dolez 31, 7000 Mons, Belgium

ARTICLE INFO

Keywords:
Fiber optic biosensor
Gold electroless plating (ELP)
Tilted fiber Bragg gratings (TFBG)
Plasmonic sensing
Cytokeratin-17 detection

ABSTRACT

In the context of plasmonic sensing using optical fibers, the controlled deposition of thin metal films remains a challenge, especially because of their cylindrical shape. In this work, we study the gold electroless plating (ELP), which is a direct and cost-effective technique to improve the quality and reproducibility of the metal deposition. In this paper, we use optical fibers to monitor the deposition process in real time. Our analysis is conducted on gratings photo-imprinted in the fiber core. Using polarized light, we show how the comb-like amplitude spectra of tilted fiber Bragg gratings (TFBGs) evolve depending on the ELP duration. This spectral evolution linked to a thorough study of the metal surface allows us to define the optimized process for improved surface refractometry. We experimentally show that this happens for a particular arrangement of gold nanoparticles yielding spectral features comparable to those obtained for localized surface plasmon resonance (LSPR) excitation. Biosensing experiments were performed and a LOD of 1 ng/mL (14 pM) is reported. This comes along with an enhanced specificity, contrasting with a poor sensitivity to bulk refractive index. All this is paving the way to a fast online coating procedure for nano-scaled and label-free biosensing using optical fibers.

1. Introduction

Surface Plasmon Resonance (SPR) biosensors are sensing devices, which consist of a metal-dielectric interface on which selected biomolecules (proteins, antibodies, DNA, enzymes, lipids, carbohydrates, cells, etc.) are grafted to interact with specific analytes [1]. The metal layer can be a continuous film (or sheath) or an array of nanoparticles. This second configuration usually leads to the excitation of localized surface plasmon resonance (LSPR), which is known to be more sensitive to near-surface interactions [2]. These devices also need a transducer, translating binding events into a readable signal [3].

Plasmonics is a widespread technology among biosensors and is used in different fields of analysis (safety detection, environmental monitoring, disease or cancer diagnosis, food control, etc.) [4,5]. Its label-free detection and real time monitoring are important characteristics compared to classical bio-recognition techniques (e.g. ELISA, PCR, and other immunological techniques) [6]. This sensing technology is most often used with the Kretschmann configuration, especially for the commercially available BIACORE system released in 1990, but it has been demonstrated that SPR can also be transposed to optical fibers (OF) [7–9].

The use of OF as biosensors is intriguing because they offer a lot of assets [10]. Their flexibility, thickness, reliability, ease of light injection and relative low cost are among their most relevant qualities [11]. Moreover, the current optical methods available for chemical analyses rely on an enormous background making experiments quick and accurate, in large part thanks to high-performance optical interrogators [12,13].

Numerous optical fibers configurations can be used for biosensing purposes, such as unclad optical fibers [14], bend or etched fibers [15,16], side-polished fibers [17], long period fiber gratings (LPFGs) [18] and fiber Bragg gratings (FBGs) [19]. Different sensing modalities can be used as well. In addition to (L)SPR, the use of lossy mode resonance (LMR) or the intrinsic properties of the optical transduction without metal coating gains in interest [20–22].

In this paper, our selected key enabling technology is the use of permanent gratings photo-inscribed into the core of fibers. It has been demonstrated that such gratings bring valuable advantages for practical implementations: tuning of the SPR mode excitation wavelength via selective cladding mode coupling, subsequent compatibility with telecommunication-grade optical fibers and equipment, temperature self-compensation, fiber integrity conservation and compatibility with mass production, among others [23,24]. Within all the possible grating architectures, tilted fiber Bragg gratings (TFBGs) intrinsically enable

* Corresponding author.
E-mail address: christophe.caucheteur@umons.ac.be (C. Caucheteur).

https://doi.org/10.1016/j.snb.2018.09.115
Received 3 April 2018; Received in revised form 25 September 2018; Accepted 26 September 2018
Available online 10 October 2018
0925-4005/

these modalities.

TFBGs are permanent refractive index modulations of the core, angled by a few degrees relatively to the perpendicular to the OF propagation axis, that couple light from the core to the cladding [25,26]. A second step is the deposition of a thin metal film at the interface between this cladding and the surrounding medium, in order to obtain plasmons excitation. However, the SPR phenomenon can only be achieved under precisely defined optical, electronic and geometric conditions. It also depends on the metal layer thickness, which is critical for precise and quantitatively reliable measurements [27].

This principle leads to highly sensitive devices, which respond to refractive index changes at the interface between the metal and the dielectric medium. In brief, TFBGs couple some wavelengths of light from the core to the cladding, making possible surface plasmon excitation. Following a biochemical surface functionalization, their amplitude spectra give information about targeted interactions, due to specific biomolecular bonds. This near-IR SPR and TFBG combination leads to a practical tool, usable for a large range of molecular interactions [28].

In recent years, it has been demonstrated that the optimum thickness of the gold film deposited for SPR on planar surfaces is ~50 nm [29]. Using this configuration adapted to optical fibers, it is possible to obtain narrow SPR extinction and as a result, high-sensitivity biosensing. This leads to their use as robust biosensors in liquids [30,31] but also in non-liquid matters with a very low limit of detection (LOD), making them interesting for early and real-time disease diagnosis, as shown in our previous work [32].

The morphological properties of gold films immobilized on optical fibers play a crucial role to acquire an accurate and sensitive SPR response. When using a sputter-coater, it is not straightforward to determine the metal thickness deposited on the optical fiber. Its monitoring is often performed by online-recording quartz microbalances (QCM) that need precise calibration and do not necessarily reflect the actual thickness on the fiber, as they do not account for variations relative to the samples position into the vacuum chamber. Moreover, while a single-side deposition is possible [33], optical fibers are usually rotated by 180° to ensure a relative thickness uniformity all along the TFBG cross-section. This could be better obtained with an automatic rotation system [34]. Last but not least, the equipment needed to deposit gold (usually sputter-coater or evaporator) is very expensive and cumbersome, which is at odds with the low cost and practical aspects of optical fiber devices.

All this makes the electroless plating (ELP) gaining interest, due to its flexibility and relative ease of implementation, with extremely low cost equipment. The direct electroless deposition involves different simultaneous reactions in a metallic plating solution, without the need for external power contribution (e.g. an electric current in case of electrochemical plating). A reducing agent is only needed to transform Au^{3+} into Au° by electronic transfer, making the deposit of thin gold films possible [35].

$$2\,HAuCl_4 + 6\,NH_2OH \rightarrow 2\,Au(s) + 8\,HCl + 3\,N_2 + 6\,H_2O$$

However, noble metals as gold or silver do not attach well to glass. To enhance their adhesion, different methods have been developed, such as: interlayer deposition of Chromium or Titanium [36], the use of bifunctional links or adhesive molecules [37], and ion beam bombardment [38]. The most spread technique is the molecular linking performed by a pre-silanization of the glass substrate. It is also the only process adapted for optical fibers without the need for specific device.

In comparison with the sputtering deposition, several practical issues are solved with ELP: vacuum intensity variations, samples position changes, and the wear of the gold target that can affect the coating efficiency. Moreover, the ELP is very fast and flexible, because it can be prepared and performed in a few minutes, and easily adapted for different materials, which is a key point to manufacture micro devices and biosensors, among others.

ELP is mainly used for nickel, silver and copper depositions [39]. It is also actively studied for conductive films researches [40,41], SERS substrates [42] and the development of microelectrodes [43]. Of course, ELP suffers from some limitations (substrates have to be thoroughly cleaned, gold plating baths have short lifetimes, and the plating is highly sensitive to numerous conditions such as temperature, stirring effects, pH variations, etc.) but they are very minor compared to the many advantages that it brings [44]. Recent studies have also demonstrated the growing interest of gold nanoparticles (AuNPs) for chemical and biological sensing with optical fibers [45].

In this work, we have studied and optimized the ELP for TFBG-based biosensing. The originality of our approach is that the OF, connected to a polarizer and a light analyzer, can be used to monitor surface changes in real time [46]. We characterize the evolution of the TFBG orthogonally-polarized transmitted amplitude spectra as a function of ELP duration. A scanning electron microscopy (SEM) analysis was also performed to determine the corresponding metal surface morphology and thickness, allowing us to determine the optimized nanoparticles arrangement for enhanced near-interface sensitivity. Using polarization dependent loss (PDL) measurement as a read-out technique, we show that this peculiar gold nanoparticles configuration yields LSPR-like spectral features. The latter are monitored for cancer biomarkers sensing when receptors are grafted on the metal surface. Bulk and surface refractometry experiments were then conducted, revealing a poor response to bulk refractive index changes, contrasting with improved surface sensitivity and specificity for biosensing purposes. We believe that this experimental approach is paving the way to a relevant coating procedure for nano-scaled and label-free biosensing using optical fibers, which could be further optimized for imaging purposes.

2. Material and methods

2.1. Materials

Dithiolalkanearomatic-PEG_6-COOH (S_2-PEG_6COOH) came from SensoPath Technology. N-Hydroxysuccinimide (NHS); N-(3-Dimethylaminopropyl)-N'-Ethylcarbodiimide Hydrochloride (EDC); Fetal Bovine Serum (FBS); Phosphate Buffer Saline (PBS); (3-aminopropyl)trimethoxysilane 97% (APTMS); Sulfate hydroxylamine ($(NH_2OH)_2.H_2SO_4$); Lithium chloride (LiCl); 10 nm diameter gold nanoparticles in citrate buffer (AuNPs) and Gold(III) chloride trihydrate ($HAuCl_4.3H_2O$) were purchased from Sigma-Aldrich. Anti-Cytokeratin 17 antibodies (AbCK17) and Cytokeratin 17 full human Protein (CK17) came from Abcam. Bovine Serum Albumine (BSA) was purchased from Acros Organics. All buffers were prepared freshly in deionized water and protein solutions were prepared in PBS at pH 7.4 and preserved at 4 °C until experiments.

2.2. Fiber gratings photoinscription

Telecommunication-grade optical fibers (SMF-28, Ø125 µm uncoated monomode silica OF, Corning) were used to connect each sensor. Photosensitive optical fibers (PS-1250) were inserted into the NORIA (NorthLab Photonics), a grating-manufacturing equipment using a deep ultraviolet pulsed excimer laser (Coherent Excistar XS 500 Hz-ArF at 193 nm). The grating inscription was monitored in real time using an optical interrogator (FiberSensing, BraggMeter). 7° tilted TFBGs were prepared using a 1090 nm uniform phase-mask with 500 mJ laser energy and ~20,000 bursts at 50 Hz.

2.3. Thermal annealing

A thermal annealing at 200 °C was performed during two hours on ELP-TFBGs to change the gold morphology on their surface. The annealing experiments were conducted using a thermal resistance coiled around the grating location, heating at a constant temperature. Optical

fibers were then rinsed with absolute ethanol and dried under N_2.

2.4. Gold electroless plating

TFBGs were first cleaned using a piranha solution (70% H_2SO_4: 30% H_2O_2) at RT during 10 min. Then, they were rinsed with deionized water and immersed into APTMS 1% in methanol during 20 min. After that, TFBGs were rinsed with methanol and dried in the oven during 15 min at 80 °C. They were placed into 10 nm AuNPs commercial solution during 1 h at RT and rinsed with deionized water. After that, they were immersed in the ELP plating bath containing 3 mM $HAuCl_4.3H_2O$ and 0.4 mM $NH_2OH.H_2SO_4$ in deionized water. Fibers were connected to an optical analyzer and the plating time was determined from the TFBG spectral evolution.

2.5. Surface bio-functionalization

The ELP-TFBGs were functionalized with anti-CK17 antibodies according the following procedure. First, the Au films were cleaned with a brief rinsing in absolute ethanol. Then, optical fibers were immersed in 2 mM alkanethiols solution in methanol during 16 h at RT to obtain a molecular self-assembled monolayer (SAM). The sensors were then rinsed with absolute ethanol again and placed into a NHS 0.1 M/ EDC 0.5 M solution diluted in deionized water during 1 h at RT. After that step, the fibers were functionalized with anti-CK17 antibodies in a 20 µg/mL solution (PBS, pH 7.4) during 1 h30 at RT. Then, they were rinsed in PBS and directly placed in 5% BSA (w/v) in PBS, used as blocking agent during 1 h30 at RT. They were then gently rinsed again in PBS and stored in dry conditions at 4 °C (up to max. 2 weeks until experiments) (Fig. S1).

2.6. Confocal microscopy

The presence of antibodies on the surface of the ELP gold films was confirmed using the same protocol mentioned in Fig. S1, but replacing anti-CK17 antibodies by fluorescent-tagged antibodies (Ab-FITC). The fibers were then cut and fixed on glass slides, after adding a drop of VectaShield. The samples were then observed using a confocal microscope (Olympus FV1000).

2.7. Dotblot

The specificity of the anti-CK17 antibodies was tested using a Dotblot. Different proteins were immobilized on a nitrocellulose membrane (CK17, CK7 and BSA) using dots of 1.8 µL (0.2 µg/dot). The membrane was then blocked using a BSA 3% solution during 40 min in TBS-Tween 0.1% buffer (pH 7.5) at RT. Then, the membrane was immersed into an anti-CK17 antibodies solution (1:500) in BSA 5%/TBS-T buffer during 30 min under stirring. Then, the membrane was rinsed and immersed in a solution of anti-rabbit HRP antibodies (1:5000) in TBS-T/BSA 5% during 30 min. Finally, the membrane was rinsed 3x and revealed using a luminol kit + H_2O_2 by chemiluminescence (using MyECL Imager).

2.8. Bulk refractometry

Optical fibers were immersed into LiCl solutions at different concentrations (RI 1.3452–1.3600) and the wavelength shifts (nm) were measured using the most sensitive cladding mode resonances in transmitted amplitude spectra of the gratings.

2.9. Biodetection measurements

Reflection measurements were recorded with a MicronOptics interrogator (embedded in a National Instruments PXI platform) and optical fibers were connected to a light polarizer. The extremity of the TFBG was cleaved and a mirror was added using a silver glue (Fig. S2a). The sensors were then immersed into target solutions containing growing concentrations of cytokeratin 17 proteins (CK17).

Transmission measurements were recorded with a LUNA optical vector analyzer. Optical fibers were connected on each side to the interrogator thanks to pigtails. The sensitive area was fixed using magnetic clamps to the analysis position. The samples were then deposited successively on the sensitive area (Fig. S2b).

2.10. Data analysis

The data acquisition was performed through MicronOptics and Luna software combined with an automatic data saving script (in-house developed under LabView 7.0). The data analysis was performed with Origin 9.0 (OriginLab, Northampton, USA) and focused on the most sensitive modes among the spectral comb [23]. Baselines variations and Bragg Peak variations were compensated for each analysis. The amplitude variations were then calculated for each tested conditions and for each sensor. The first experiments in PBS were considered as the initial amplitude values regarding to further proteic solutions. Statistical analyses were performed through Origin 9.0 and R-studio.

2.11. SEM analysis

Optical fibers recovered by ELP were analyzed by SEM. OF were cleaved and glued on stubs. They were then observed at different magnifications (JEOL JSM 7200F). EDX measurements were also performed to determine the nature of the focused substrate. The thickness of gold layers was established with cleaved OF glued perpendicularly to the stub, when nanoparticles sizes and morphologies were determined on longitudinally glued OF. A percentage of gold coverage was calculated through a MATLAB script: the SEM images were standardized and converted by image contrast into white and black matrices. Then, the script calculated the number of white and black pixels, respectively. The threshold was adjusted using 100% black, 100% white and 50% w/b patterns (Fig. S3).

3. Results and discussion

The main aim of our experimental study was to optimize ELP protocols to optical fiber gratings for highly-sensitive surface biosensing. To this aim, different plating conditions were tested in small volumes to obtain fast and reproducible plating for nm-scale layer thickness. In each case, polarization-assisted spectral measurements and SEM analysis were conducted jointly, allowing to define the best plating conditions for our objective. In the following, we first present the SEM analysis in Section 3.1 and then the spectral characterizations in Section 3.2. It is important to mention that in our approach both analyses have to be correlated. Sensing experiments are then reported in Section 3.3.

To conduct the ELP process, the target surface (made of silica activated with APTMS 1% and 10 nm gold nanoparticles) was immersed into the plating solution containing the metal ions (Au^{3+}) and the reducing agent (hydroxylamine) at the same time. A gold film deposition only happens if the electronic transfer from the reducer to the metal is slow. Otherwise, all the metal would be reduced into the plating solution after few seconds and provoke the apparition of black precipitates.

Furthermore, the use of hydroxylamine is known to highly accelerate the reduction onto the gold nanoparticles. This hydroxylamine-accelerated reduction of Au^{3+} is also known to increase the size of these already immobilized AuNPs, avoiding production of new nucleation sites [47].

3.1. SEM analysis of ELP surfaces

A SEM study of the ELP surface was performed to characterize its morphology and its homogeneity. Different reaction times of ELP

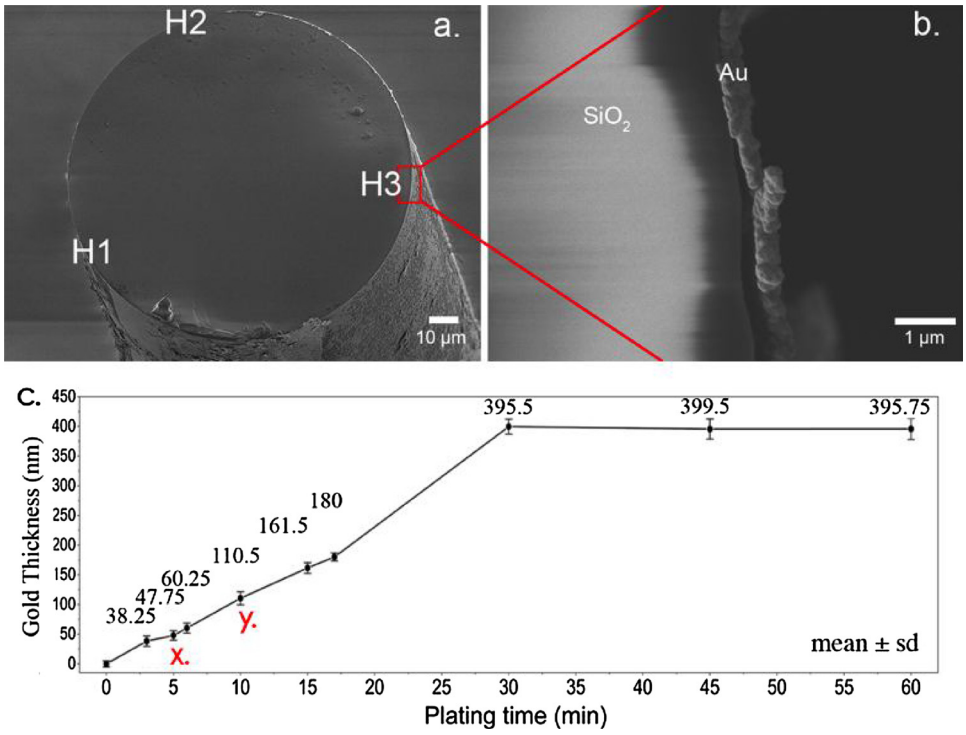

Fig. 1. SEM images of the gold layer deposited around the fiber surface after a silica pre-silanization. The height (mean ± sd) was calculated through 3 different equitably distributed positions H1, H2 and H3 on each fiber (a). Zoom around the H3 position (b). Graph showing the evolution of the gold layer thickness depending on plating time. This thickness evolution was measured by SEM after ELP on optical fibers (mean ± sd) (c).

process were tested to investigate its impact on the gold films. Some OF were glued perpendicularly on the support to analyze the thickness of the layer deposition. This method allowed us to estimate the films thicknesses in real conditions after each experiment, as illustrated in Fig. 1a, b.

Fig. 1c gathers the results obtained for 9 different ELP times ranging between 3 and 60 min. It shows the thickness evolution, computed according to the aforementioned method as a function of plating time. A gold layer thickness of 110.5 ± 12 nm was observed after 10 min of ELP with a concentration of 3 mM $HAuCl_4$ and 0.4 mM $(NH_2OH)_2{\cdot}H_2SO_4$, when only ~35 nm layers were highlighted in the same conditions after 3 min. We also noticed that a maximum of ~400 nm was reached in that plating conditions, considered as the complete use of gold ions present in the plating bath, from 30 min of deposition. After that time, the metal deposition ends and the thickness does not evolve anymore.

Fig. 2a and b show the SEM images of the plated surfaces obtained after 3 and 10 min of ELP (marked *X* and *Y* on Fig. 1b). They confirm that the morphology of gold particles changes during the process, progressively switching from spherical and hexagonal shapes to more complex associations. For comparison, Fig. 2c shows a ~35 nm thick sputtered gold surface, underlining a strong difference with ELP surfaces. The sputtered surfaces show an obvious lack of granularity, which is therefore more difficult to analyze with a SEM approach.

Indeed, ELP consists of progressively growing gold plates, forming a layer after using the pre-immobilized gold nanoparticles as nucleation sites. The surface is then wavier in comparison with plasma-sputtered surfaces and only becomes more uniform after a sufficient plating time, when particles are big enough to merge together. We also noticed that in our conditions, the surface is more homogeneous after 10 min of plating, when higher plating times provoke the formation of bigger gold clusters and precipitated salts, decreasing the fair distribution of gold particles among the fiber.

The surface covering also increases as a function of time. To calculate the percentage of coverage, we analyzed SEM images with a MATLAB script. After a black and white transformation of the SEM images, plated areas were represented in white while silica areas remained black. The sum of white pixels divided by the total of the pixels for each image gave us an approximation of the plated area (Fig. S3). This investigation showed that 3 min of ELP was enough to functionalize 72.5% ± 4.5% of the surface when, after 10 min, the gaps between growing gold clusters became negligible, with a coverage of 93.2% ± 5.03%, as summarized in Fig. 2d. In consequence, it is necessary to end the reaction after around 3 min of plating to preserve the inhomogeneous nature of the gold nanoparticles organization, which is essential for highly sensitive surface sensing, as demonstrated in the following.

3.2. Spectral analysis of ELP-TFBGs

To complete this ELP study, TFBGs were connected to the interrogator and the signal was monitored during the deposition (Fig. S2). Thanks to their high signal-to-noise ratio, they are appropriate tools to monitor thin films deposition in real time and evaluate the metal thickness by correlating their associated spectra [48].

A complete and progressive disappearance of all the IR-light modes in the transmitted amplitude spectra was observed until 3 min of plating, corresponding to 35 nm of gold immobilized on the fiber surface. This extinction of the cladding modes was correlated with growing Au particles on the silanized surface, provoking an enhanced light scattering into the plating solution. Only few seconds after this total modes disappearance, they began to return gradually to their initial amplitude, due to the increasing gold layer, acting this time as a mirror and preventing light to escape from the fiber cladding, yielding a strong sensitivity decrease (Fig. 3a).

To finely investigate the spectral modifications linked to the gold formation, a more sensitive polarization parameter was then considered, as initiated before in [46]. This is the so-called polarization dependent loss (PDL) spectrum that corresponds to the absolute difference between the orthogonally-polarized spectra of the grating. This parameter is directly computed by the OVA. Interestingly, the PDL spectrum depicts a local attenuation of the cladding mode resonances centered on ~ 1572 nm with 35 nm of gold, as depicted in Fig. 3b. This plating time corresponds to the surface morphology reported in Fig. 2a where gold nanoparticles begin to coalesce but with sufficient gaps in between, as the total surface coverage is ~75%. The resonances

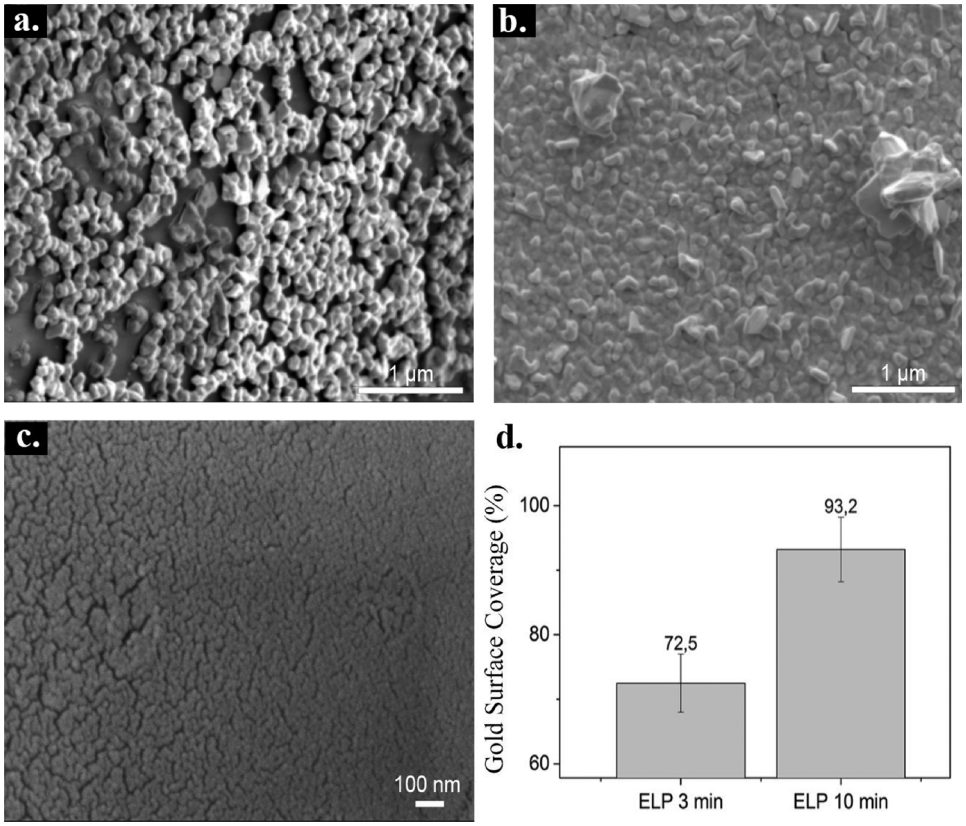

Fig. 2. SEM surface morphology after 3 min (a) and 10 min of ELP (b). SEM image of a 35 nm gold layer deposited by plasma sputtering on optical fiber (c). Graph showing a percentage of gold coverage (mean ± sd) (d).

affected by this local PDL attenuation are strongly sensitive to surface refractive index changes, as demonstrated in the following. Hence, this behavior tends to prove that this peculiar gold morphology yields LSPR-like generation due to collective effects between agglomerated nanoparticles. This induces a shift from the visible to the near-infrared wavelength range together with a spectral enlargement due to scattering effects. In these conditions, the LSPR-like excitation can be probed by the grating resonances.

To support our explanations, we have conducted a thermal annealing process to change the morphology of the gold surface, as reported in the literature [49,50]. A temperature of 200 °C was chosen, to avoid damaging the inner fiber core grating while inducing an effective impact on metal films.

As shown in Fig. 4a and b, results demonstrate that a thin gold ELP

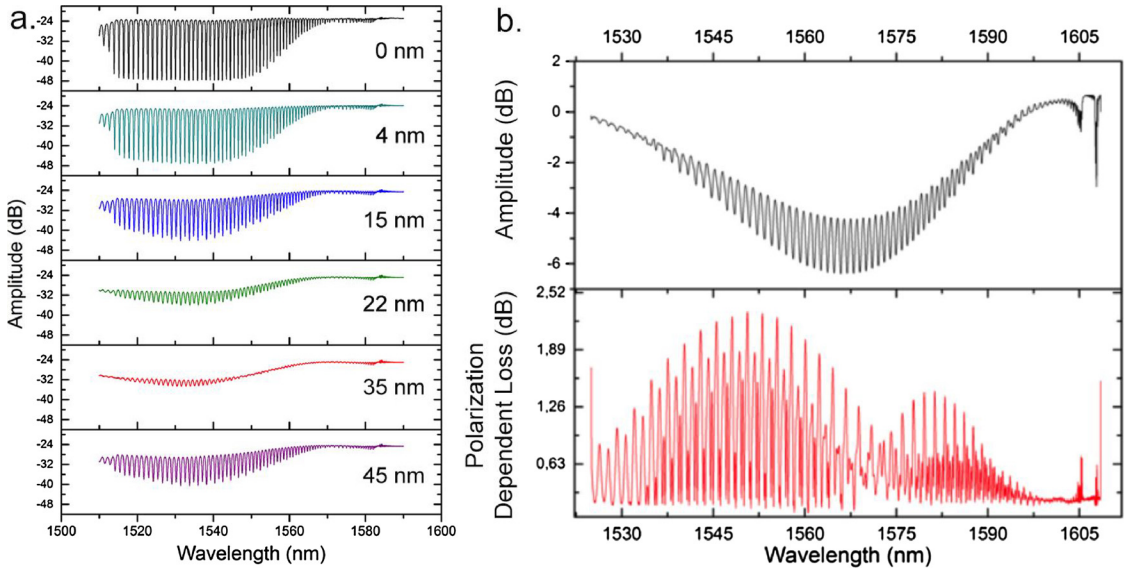

Fig. 3. Evolution of the TFBGs transmitted amplitude spectra until 4 min of ELP, from 0 to 45 nm of gold at the end of experiment. The light scattering phenomenon is the most intense with a gold thickness of ~35 nm (a). Graphs showing the Insertion Loss (dB) in black, and the Polarization Dependent Loss (dB) in red for the same TFBG, in transmission after 3 min of ELP with ~35 nm of gold (b). (For interpretation of the references to colour in this figure legend, the reader is referred to the web version of this article).

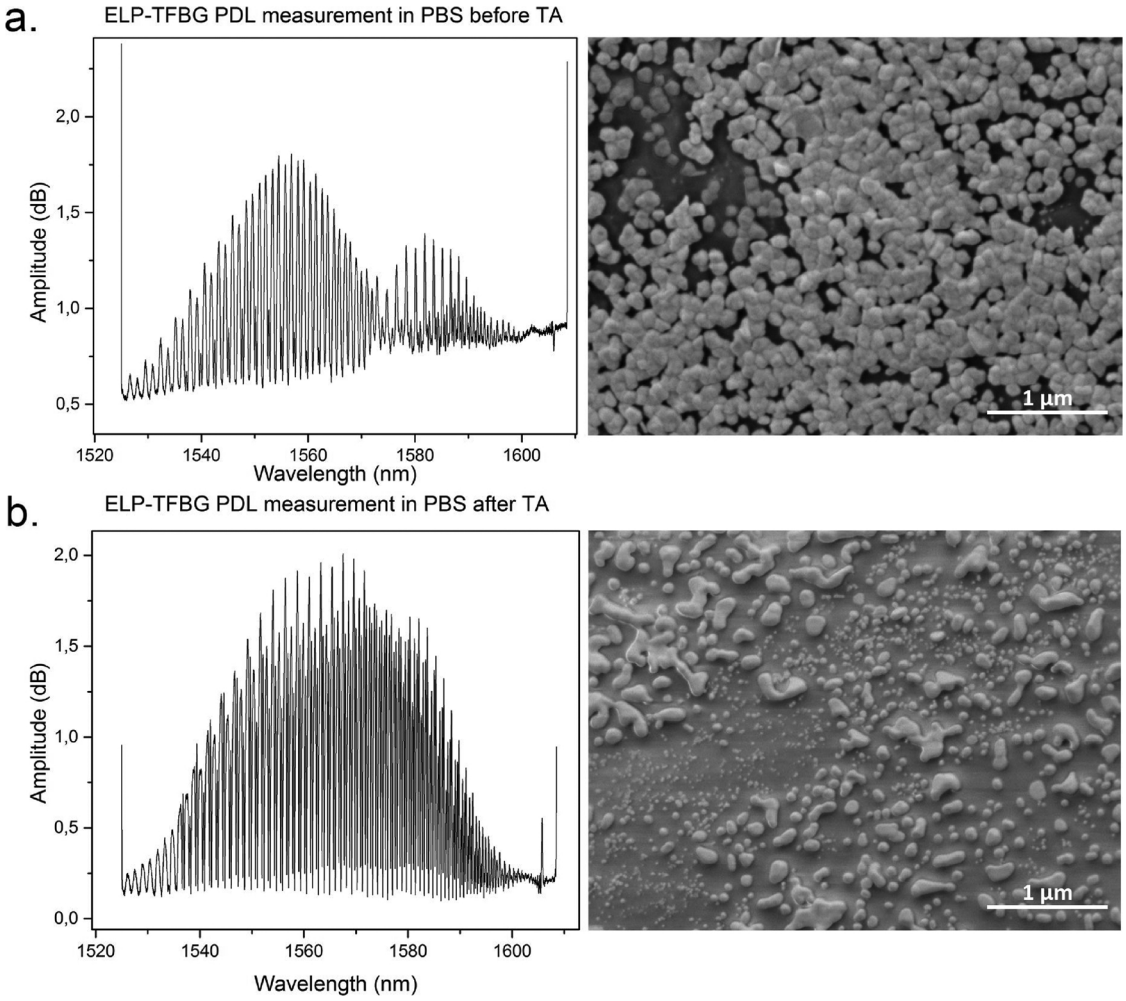

Fig. 4. Graph showing the ELP-TFBG PDL measurements in transmission before thermal annealing, where the gold coverage is about 73.5% out of the entire fiber surface (a) and for the same fiber after 2 h of thermal annealing at 200 °C, where gold covers all the fiber surface (b).

film heating provokes its reorganization and induces a smoothing of the immobilized nanoparticles. Using the same image processing as for the previous SEM study, we observed that a 2 h thermal annealing at 200 °C causes important changes in terms of gold particles shapes. Also the surface coverage passes from ~73.5% to ~100% for the optimized plating time. Light scattering is therefore prevented and the PDL spectrum depicts its characteristic Gaussian shape (Fig. 4b).

All these results confirm that an efficient gold coating process should last ~3 min to obtain the extinction signature. Furthermore, this duration is adapted for a live spectrum monitoring on the one hand, and faster compared to other processes, on the other hand.

3.3. Sensing experiments

3.3.1. Bulk refractometry

An important sensing application of TFBGs is refractometry. To quantify the sensitivity of our sensors to global refractive index variations, ELP optical fibers were immersed into successive lithium chloride concentrations (the refractive index variations were controlled in parallel with a refractometer).

The wavelength shifts of the most sensitive light modes were then reported for each concentration as a function of the surrounding refractive index change. This test allowed us to determine the bulk sensitivity using the following equation:

$$Sensitivity\ (nm/RIU) = \frac{\Delta\lambda\ (\boldsymbol{nm})}{\Delta \boldsymbol{RI}\ (\boldsymbol{RIU})}$$

It is worth mentioning that most of people working with TFBGs use wavelengths shifts to quantify bulk refractometry, while our team most often use amplitude shifts to monitor biosensing experiments. To allow comparison with other studies, we show the RI sensitivity in nm/RIU, as the convention requires.

Our ELP-TFBGs sensors present a low RI sensitivity, reaching a maximum of only 9.88 nm/RIU (Fig. 5) or 59.3 dB/RIU in amplitude. For instance, bare-TFBGs present a bulk sensitivity of ~ 25 nm/RIU, which is still very small in comparison with long period gratings (LPGs) that can reach about 10^4 nm/RIU [51].

This very low sensitivity observed for bulk effect confirms the hypothesis of LSPR-like spots within the ELP film. Indeed, the depth of the analysis field is decreasing and the gold nanostructures play here a role of “bulk-fence”, which could be further exploited for highly specific measurements in rich environments such as blood or physiological samples, where the concentrations of analytes can modify the RI and therefore impinge the sensor specificity.

Our results are contrasting with some experiments reported in literature, based on higher annealing temperatures (up to 900 °C) and thinner gold films (5 nm) deposited by traditional methods such as sputtering, and showing a RI sensitivity around 500 nm/RIU [52]. Therefore, the innovation of our approach, in addition of the deposit method, exactly lies in this global RI loss of sensitivity to avoid unspecific signal response in complex media.

We recall that our goal was to use this gold film thickness to maintain the sensor barrier-effect avoiding nonspecific responses, while

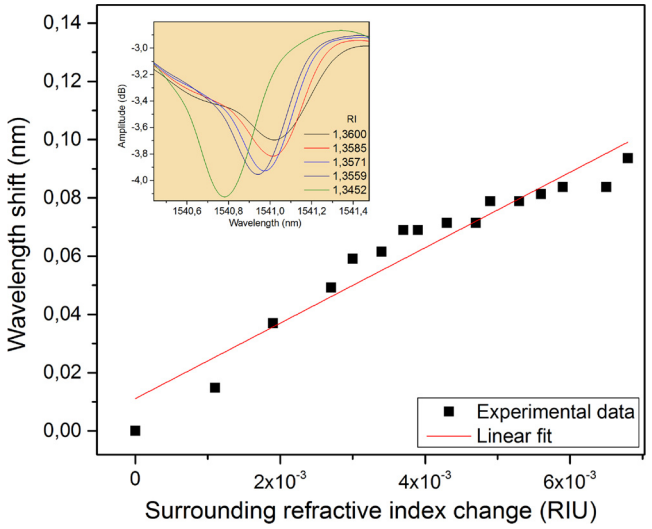

Fig. 5. ELP-TFBG wavelength shifts of the most sensitive mode of the spectra, measured in PDL for different surrounding refractive indexes. (Linear fitting, slope = 12.90 ± 0.98 R^2 = 0.919).

reaching a higher surface sensitivity for biosensing performances.

3.3.2. *Surface refractometry: cytokeratin detection*

The impacts of the metal deposition on the biosensitivity and specificity were studied through laboratory settings, using the Cytokeratin 17 protein (CK17) as target. This protein was recently studied in our lab as a potential lung cancer biomarker, showing growing interest for fiber optic biosensing in case of early in situ diagnosis.

First, a confocal microscopy experiment confirmed the correct antibodies immobilization on the ELP gold layers using FITC-tagged antibodies while negative control fibers without linking agents between the fiber surface and the antibodies showed no fluorescence (Fig. 6a).

A dotblot was also performed on a nitrocellulose membrane to test the specificity of the anti-CK17 antibodies and to prove the non-interaction with close proteins (CK7) or with fetal bovine serum albumin proteins (BSA) present in FBS during sensing experiments (Fig. 6b).

The biosensing responses were then studied consecutively using ELP-TFBGs functionalized with anti-CK17 antibodies in first; PBS buffer solutions as reference responses; then into PBS + Fetal Bovine Serum 1% to test the specificity of the sensors; and finally into three growing concentrations of CK17: PBS + FBS 1% + CK17 10^{-12} g/mL; 10^{-9} g/mL and 10^{-6} g/mL, respectively. The responses were monitored through amplitude variations located to the most sensitive modes, near the SPR attenuation area of the spectra. Five different fibers were tested in these successive conditions during 5 min for each concentration (Fig. 6c).

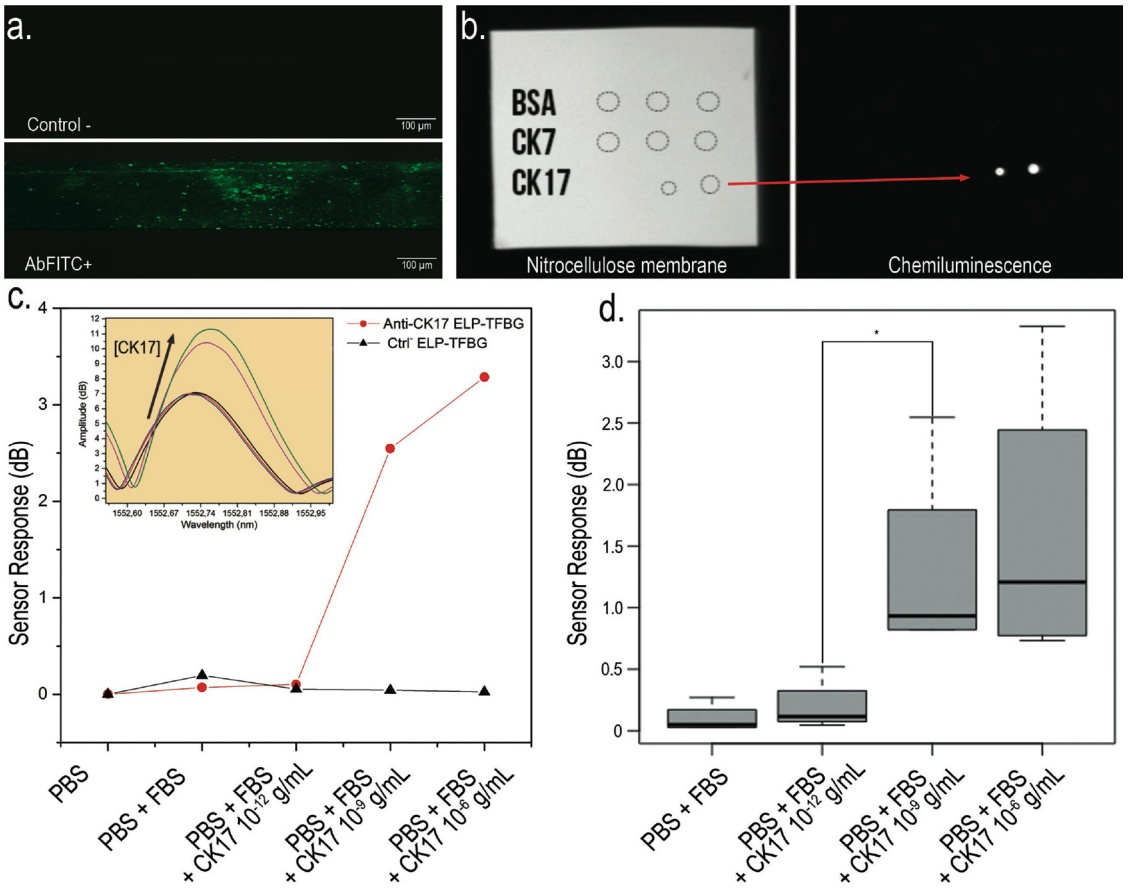

Fig. 6. Confocal microscopy images of ELP control OF without linking agent, and of functionalized ELP-OF with FITC-labeled antibodies (a). Pictures of Dotblot realized on a nitrocellulose membrane to verify the specificity of the anti-CK17 antibodies (b). Graph showing the evolution of the ELP biosensor response after 5 min in successive conditions, from PBS to PBS + FBS 1%, and then into growing CK17 concentrations for one experiment. The red curve shows the response of an anti-CK17 functionalized ELP-TFBG while the black curve shows the response of a negative control fiber, without immobilization of anti-CK17 antibodies (c). Paired *t*-test boxplot realized with 5 different anti-CK17 optical fibers, showing the signal evolution between each condition from PBS + FBS 1% to the highest CK17 concentration tested. A significant signal variation (*) was observed for the transition between CK17 10^{-12} g/mL and 10^{-9} g/mL what also corresponds to the limit of detection (LOD) of the sensor (p-value < 0.05) (d). (For interpretation of the references to colour in this figure legend, the reader is referred to the web version of this article).

The first test comparing the initial measurement in PBS (RI = 1,3345) and PBS + FBS 1% (RI = 1,3353) shows no significant variation even if there is a significant RI change. Actually, TFBGs are highly sensitive to RI variations but the ELP gold film decreases the bulk sensitivity, as explained before. The sensor is more sensitive on the surface located area, increasing its specificity by decreasing the global refractive index variation impact.

When changing the solution from PBS to CK17 10^{-12} g/mL, which was the lowest concentration tested, no significant variation happened. However, from 10^{-9} g/mL, a significant amplitude variation occurred in only few seconds, proving the detection potential of this new ELP-sensor with a low limit of detection of 1 ng/mL (14 pM). Then, the sensor showed again less important signal variations when reaching a higher proteic concentration (Fig. 6d). This can be linked to the ELP surface morphology and/or to the surface saturation due to the repeated tests with growing CK17 concentrations. The dispersion between the reference signal and the one measured in PBS + FBS is smaller that the one achieved before for continuous gold sheaths [53], pointing out an additional benefit of our method.

Finally, these immunosensing experiments have successfully demonstrated the possibility of detection using this new ELP-TFBG configuration, making it relevant for targeted protein detection in complex media. This can be particularly relevant for new fiber-optic based diagnosis tests, such those developed to enter in contact with blood, urine, or tissues that need high specificity to avoid false positive or false negative detection. As we immobilized antibodies on the metal film, this sensor can also be used with other receptors such as aptamers, DNA, enzymes, etc. [10] allowing to achieve sensors more suited for complex and variable environments.

4. Conclusion

The ELP method was successfully tailored for optical fiber gratings, lowering their sensitivity to bulk refractive index while increasing their specific surface response for biosensing purposes. Our experimental approach, combining SEM analysis of the plated gold surface with polarization-assisted spectral measurements of the tilted gratings, has conducted to the demonstration of LSPR-like effects in the grating wavelength range around the telecommunication window at 1550 nm. This was achieved for a particular metal arrangement composed of coalesced nanoparticles and non-coated areas, in a ratio close to 75/25. For a given selection of reagents concentrations, the only parameter to control to achieve this was the plating time. A limit of detection of 1 ng/mL (14 pM) was established with Cytokeratin 17 detection experiments, what underlines its interesting aspect for targeted proteins sensing into complex media. Our approach resulted in a real-time and reliable protocol for TFBGs gold coating, allowing to develop a more specific detection tool for plasmonic analysis.

Funding sources

This work is supported by the F.R.S.-FNRS through a FRIA grant and an Associate Researcher grant.

Acknowledgments

This work is supported by the F.R.S.-FNRS through the EOS grant O001518F (ID EOS: 30467715). The authors thank the laboratory of Marine Biology of the University of Mons for the access to the SEM equipment, provided by Prof. I. Eeckhaut and Prof. P. Flammang.

Appendix A. Supplementary data

Supplementary material related to this article can be found, in the online version, at doi:https://doi.org/10.1016/j.snb.2018.09.115.

References

[1] P. Singh, Sens. Actuators B-Chem. 229 (2016) 110–130.
[2] K.A. Willets, R.P. Van Duyne, Annu. Rev. Phys. Chem 58 (2007) 267–297.
[3] J. Homola, Chem. Rev. 108 (2008) 462–493.
[4] K. Narsaiah, S.N. Jha, R. Bhardwaj, R. Sharma, R. Kumar, J. Food Sci. Technol. 49 (4) (2012) 383–406.
[5] V. Duyne, Proc. IEEE 104 (12) (2016) 2380–2408.
[6] S. Shi, L. Wang, A. Wang, R. Huang, L. Ding, R. Su, W. Qi, Z. He, J. Mater. Chem. C 4 (2016) 7554–7562.
[7] X. Fan, I.M. White, S.I. Shopova, H. Zhu, J.D. Suter, Y. Sun, Anal. Chim. Acta 0 (2008) 8–26.
[8] A.K. Sharma, R. Jha, B.D. Gupta, IEEE Sens. J. 7 (8) (2007) 1118–1129.
[9] I. Arghir, F. Delport, D. Spasic, J. Lammertyn, N. Biotechnol. 32 (5) (2015) 473–484.
[10] F. Chiavaioli, F. Baldini, S. Tombelli, C. Trono, A. Giannetti, Nanophotonics 6 (4) (2016) 663–679.
[11] P. Vaiano, B. Carotenuto, M. Pisco, A. Ricciardi, G. Quero, M. Consales, A. Crescitelli, E. Esposito, A. Cusano, Laser Photonics Rev. 961 (6) (2016) 922–961.
[12] B. Lee, Opt. Fiber Technol. 9 (2003) 57–79.
[13] R. Mar, D. Marazuela, C. Moreno-bondi, Anal. Bioanal. Chem. 372 (2002) 664–682.
[14] J. Pollet, F. Delport, K.P.F. Janssen, K. Jans, G. Maes, H. Pfeiffer, M. Wevers, J. Lammertyn, Biosens. Bioelectron. 25 (2009) 864–869.
[15] C. Christopher, A. Subrahmanyam, V.V.R. Sai, Plasmonics 13 (2) (2018) 493–502.
[16] S. Schulze, M. Wehrhold, C. Hille, Sensors 18 (2018) 2844.
[17] J. Zhao, S. Cao, C. Liao, Y. Wang, G. Wang, X. Xu, C. Fu, G. Xu, J. Lian, Y. Wang, Sens. Actuators B-Chem. 230 (2016) 206–211.
[18] F. Baldini, M. Brenci, A. Chiavaioli, A. Giannetti, Anal. Bioanal. Chem. 402 (1) (2012) 109–116.
[19] T. Guo, Á. González-Vila, M. Loyez, C. Caucheteur, Sensors 17 (2017) 2732.
[20] Q. Wang, W.-M. Zhao, Opt. Lasers. Eng. 100 (2018) 47–60.
[21] F. Chiavaioli, P. Zubiate, I. Del Villar, C.R. Zamarreño, A. Giannetti, S. Tombelli, C. Trono, F.J. Arregui, I.R. Matias, F. Baldini, ACS Sens. 3 (5) (2018) 936–943.
[22] M. Loyez, J. Albert, C. Caucheteur, R. Wattiez, Biosensors 8 (2018) 74.
[23] C. Caucheteur, T. Guo, J. Albert, Anal. Bioanal. Chem. 407 (14) (2015) 3883–3897.
[24] F. Chiavaioli, C.A.J. Gouveia, P.A.S. Jorge, F. Baldini, Biosensors 7 (2) (2017) 23.
[25] C. Caucheteur, V. Voisin, J. Albert, Opt. Express 21 (3) (2013) 1142–1149.
[26] J. Albert, L. Shao, C. Caucheteur, Laser Photonics Rev. 26 (2012) 1–26.
[27] H. Neff, Thin Solid Films 496 (2006) 688–697.
[28] Y. Shevchenko, T.J. Francis, Da D. Blair, R. Walsh, M.C. Derosa, J. Albert, Anal. Chem. 83 (2011) 7027–7034.
[29] J.M. Rooney, E.A.H. Hall, Anal. Chem. 76 (2004) 6861–6870.
[30] T. Guo, F. Liu, X. Liang, X. Qiu, Y. Huang, C. Xie, P. Xu, Biosens. Bioelectron. 78 (2016) 221–228.
[31] J. Lu, D. Spasic, F. Delport, T.V. Stappen, I. Detrez, D. Daems, S. Vermeire, A. Gils, J. Lammertyn, Anal. Chem. 89 (6) (2017) 3664–3671.
[32] C. Ribaut, M. Loyez, J. Larrieu, S. Chevineau, P. Lambert, M. Remmelink, R. Wattiez, Biosensens. Bioelectron 92 (2017) 449–456.
[33] D. Feng, W. Zhou, X. Qiao, J. Albert, Opt. Express 24 (15) (2016) 16456.
[34] Y. Shevchenko, J. Albert, Opt. Lett. 32 (3) (2007) 211–213.
[35] A. Lahiri, S.I. Kobayashi, Surf. Eng. 32 (5) (2016) 321–337.
[36] R. Audino, G. Destefanis, F. Gorgellino, E. Pollino, S. Tamagno, Thin Solid Films 36 (1975) 343–347.
[37] W. Chen, Y. Tseng, S. Hsieh, W. Liu, C.-W. Hsieh, C.-W. Wu, C.-H. Huang, H.-Y. Lin, C.-W. Chen, P.-Y. Linb, L.-K. Chau, RSC Adv. 87 (2014) 46527–46535.
[38] L. Guzman, A. Miotello, R. Checchetto, M. Adami, Surf. Coat. Technol. 158 (2002) 558–562.
[39] J. Hu, W. Li, J. Chen, X. Zhang, X. Zhao, Surf. Coat. Technol. 202 (2008) 2922–2926.
[40] K.R. Brown, L.A. Lyon, A.P. Fox, B.D. Reiss, M.J. Natan, Chem. Mater. 12 (2) (2000) 314–323.
[41] H. Naor, D. Avnir, ACS Appl. Mater. Interface (2015) 26461–26469.
[42] M.Y. Elsayed, A.M. Gouda, Y. Ismail, M.A. Swillam, J. Lightwave Technol. (2017) 3075–3081.
[43] K. Niitsu, S. Ota, K. Gamo, H. Kondo, M. Hori, K. Nakazato, IEEE Trans. Biomed. Circ. Syst. 9 (5) (2015) 607–619.
[44] H.O. Ali, I.R.A.A. Christie, Gold Bull. 17 (4) (1984) 118–127.
[45] S. Lepinay, A. Staff, A. Ianoul, J. Albert, Biosenens. Bioelectron. 52 (2014) 337–344.
[46] A. Bialiayeu, C. Caucheteur, N. Ahamad, A. Ianoul, J. Albert, Opt. Express 19 (20) (2011) 481–490.
[47] S. Hrapovic, Y. Liu, G. Enright, F. Bensebaa, J.H.T. Luong, Langmuir 83 (9) (2003) 3958–3965.
[48] D.J. Mandia, Z. Zhou, J. Albert, S.T. Barry, Chem. Vap. Deposition 21 (2015) 4–20.
[49] I. Antohe, K. Schouteden, P. Goos, F. Delport, D. Spasic, J. Lammertyn, Sens. Actuators B-Chem. 229 (2016) 678–685.
[50] J. Zhang, M. Irannejad, M. Yavuz, B. Cui, Nanoscale Res. Lett. 10 (238) (2015).
[51] Q. Shi, B.T. Kuhlmey, Opt. Commun. 282 (24) (2009) 4723–4728.
[52] A. Hosoki, M. Nishiyama, K. Watanabe, Appl. Opt. 56 (23) (2017) 6673–6679.
[53] C. Ribaut, V. Voisin, V. Malachovská, V. Dubois, P. Mégret, R. Wattiez, C. Caucheteur, Biosens. Bioelectron. 77 (2016) 315–322.